Improved drag coefficient modeling with spatial and temporal Fourier coefficient expansions: theory and application

Vishal Ray* and Daniel Scheeres†
University of Colorado Boulder, Boulder, CO 80309-0020

Siamak Hesar‡ and Matthew Duncan§
SpaceNav LLC, Boulder, CO 80301

The estimation and modeling of drag effects on low altitude satellites and debris is a limiting problem in the prediction of their orbits over time. Independent of the stochastic variations in atmospheric density, which drive the magnitude of the drag force, there are systematic variations in the drag coefficient due to satellite specific factors and atmospheric conditions. These include satellite attitude shifts which cause variations in projected area, variations in ambient atmospheric parameters such as temperature, molecular composition, and the satellite wall temperature. Thus, even with accurate empirical models for the atmospheric density, there remain systematic model uncertainties and time variations in the effective coefficient of drag of a body that affect its motion, which are not captured using the standard constant drag coefficient model. We report on our recent research on developing improved models of an arbitrary object's coefficient of drag with the overall purpose to develop corrections to the standard model. Our approach leverages previous research on improving solar radiation pressure models. If the attitude profile of a satellite or object is known, a Fourier Series expansion of the overall coefficient of drag as a function of wind vector direction in the body-frame can be introduced. For bodies with unknown or more complex attitude profiles, we introduce a periodically varying drag coefficient tied to a satellite's position in its orbit. This model enables the estimation of higher-order temporal variations in drag that would be correlated with variations in attitude, temperature and density. An improved prediction capability is shown with the model and the formulation of how it can be incorporated into standard Kalman filter techniques is presented.

I. INTRODUCTION

Atmospheric drag is one of the most significant perturbing forces in the Low Earth Orbit (LEO) regime. The atmospheric force on a satellite has three components - drag, lift and side forces. The lift and side force coefficients are an order of magnitude smaller than the drag force coefficients [1]. Lift forces cause radial perturbations of around 1 cm over a 5 day period which increases around tenfold during periods of high solar activity [2]. Though cross track forces will be important for very precise orbit determination, they can be ignored without significant loss in accuracy. The drag force is essentially a function of the density, the cross sectional normal to the flow and the drag coefficient (see Eq. 10). A critical evaluation of the state-of-the-art density and drag coefficient models used to calculate the atmospheric drag has been provided by [3]. The accuracy with which the drag force can be estimated is strongly tied to the atmospheric model being used to calculate the density. A comprehensive review of atmospheric density calculations and its dependence on various ambient parameters can be found in [4]. The cross-sectional area normal to the flow can be integrated into the drag coefficient. In the orbit determination (OD) process, the drag coefficient is generally estimated as a constant, similar to the cannonball model for solar radiation pressure (SRP) [5]. But the drag coefficient is dependent on satellite parameters such as attitude and the surface material as well as atmospheric parameters such as temperature and molecular composition. Therefore, the drag coefficient varies throughout the orbit as one or more of these parameters change. For precision OD, ideally the complete variation of the drag coefficient based on the physics of the flow should be modeled in the filter. But many of the parameters such as the energy accommodation coefficient, which is essentially a measure of the reemitted energy from the satellite wall, are not available with enough accuracy.

*PhD Student, Aerospace Engineering and Sciences, Boulder, Colorado, vira0155@colorado.edu
†Distinguished Professor, Aerospace Engineering and Sciences, Boulder, Colorado, scheeres@colorado.edu
‡Chief Scientist, SpaceNav LLC, Boulder, Colorado, siamak@space-nav.com
§President and CEO, SpaceNav LLC, Boulder, Colorado, matt@space-nav.com

Estimating the parameters in the filter is not possible since they have an implicit dependence on each other, rendering them unobservable. Even if estimating the parameters was possible, the models used to calculate the drag coefficient are only approximations of the actual physics that govern the flow. This calls for the need of a model that can condense the physics associated with the drag coefficient into observable quantities that can then be estimated in a filter.

Fourier series models have been used to better approximate the solar radiation pressure and the thermal radiation pressure than the standard cannonball model in previous literature [6–9]. Fourier coefficients being orthogonal to each other can be estimated in a filter. In this work, Fourier series models tied to the satellite body and orbit have been developed for the drag coefficient. The model used to generate the true drag coefficients is outlined in section II. Section III details the Fourier series model used in the filter. The simulation framework and the example cases are discussed in sections IV and V.

II. PHYSICAL MODEL

There are two existing approaches to calculate the drag coefficient - numerical and analytical. A numerical approach is generally more accurate in capturing the true drag coefficient, but analytical approaches are less computationally intensive and work well for simple shapes. Numerous gas surface interaction models (GSIMs) are available for prediction of the drag coefficient for simple shapes. In this work, a linear combination of Sentman's model [10] for diffuse reflection and Schamberg's model [11] for specular reflection has been used. The choice of these two models is based on the availability of closed form analytical expressions of drag coefficients for the geometries considered and the estimates of parameters used in these expressions from satellite measurements [12, 13]. Sentman's model has been found to closely approximate the gas surface interactions and has been used to calculate the drag coefficients in the height regime considered in this work (150-325 km) [13]. It takes into account the random thermal motion of the ambient atmosphere which becomes a crucial factor in improving the accuracy of the estimated drag coefficients as demonstrated by the comparison of density data from CHAMP and HASDM [14]. But Sentman's model is based on the assumption of a purely diffuse reemission. Though it is known that at lower altitudes with higher surface contamination, the reemission is nearly diffuse and it becomes quasi-specular for higher altitudes, the transition is not well defined or modelled. Instead of using two separate models for the two regimes, we attempt to model the transition using a linear combination of models [15] applicable for the two types of reemission with the weight governed by the accommodation coefficient which directly depends on the nature of reemission. The energy accommodation coefficient is modeled using the semi-empirical satellite accommodation model (SESAM) [16].

III. ESTIMATION MODEL

A. Body fixed Fourier coefficients

It can be seen that the drag coefficient is strongly dependent on the angle between the flow unit vector and the area vector of the satellite face and hence the attitude of the satellite. If the attitude of satellite is known as is mostly the case with functioning satellites, the drag coefficient variation with attitude can be potentially estimated during the orbit determination (OD) process. The unit vector of the flow can be expressed in terms of an azimuthal angle (θ) and elevation angle (ϕ) in the body frame as (Fig. 1),

$$\hat{\mathbf{u}} = \cos\phi\cos\theta\hat{x}_b + \cos\phi\sin\theta\hat{y}_b + \sin\phi\hat{z}_b. \tag{1}$$

Therefore, the drag coefficient now becomes a function of θ and ϕ which allows us to expand the drag coefficient as a double Fourier series around θ and ϕ. The double Fourier series expansion is given by, [17]

$$\begin{aligned} C_d = \sum_{m=0}^{\infty}\sum_{n=0}^{\infty} \lambda_{mn}(&\bar{A}_{mn}\cos m\theta\cos n\phi + \bar{B}_{mn}\sin m\theta\cos n\phi \\ &+ \bar{C}_{mn}\cos m\theta\sin n\phi + \bar{D}_{mn}\sin m\theta\sin n\phi) \end{aligned} \tag{2}$$

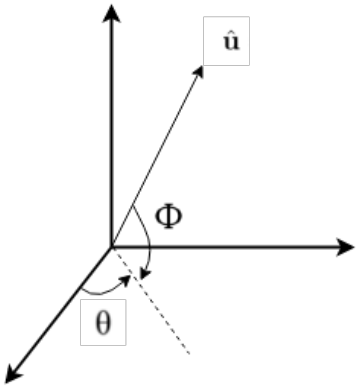

Fig. 1 Flow unit vector in body frame

where the coefficients are found as,

$$\bar{A}_{mn} = \frac{1}{\pi^2}\int_{-pi}^{pi}\int_{-pi}^{pi} C_d \cos m\theta \cos n\phi d\theta d\phi \tag{3}$$

$$\bar{B}_{mn} = \frac{1}{\pi^2}\int_{-pi}^{pi}\int_{-pi}^{pi} C_d \sin m\theta \cos n\phi d\theta d\phi \tag{4}$$

$$\bar{C}_{mn} = \frac{1}{\pi^2}\int_{-pi}^{pi}\int_{-pi}^{pi} C_d \cos m\theta \sin n\phi d\theta d\phi \tag{5}$$

$$\bar{D}_{mn} = \frac{1}{\pi^2}\int_{-pi}^{pi}\int_{-pi}^{pi} C_d \sin m\theta \sin n\phi d\theta d\phi. \tag{6}$$

The value of λ_{mn} is given by,

$$\lambda_{mn} = \begin{cases} \frac{1}{4}, & m = n = 0 \\ \frac{1}{2}, & m > 0, n = 0, \text{or}, n > 0, m = 0 \\ 1, & m > 0, n > 0. \end{cases} \tag{7}$$

B. Orbit fixed Fourier coefficients

Along with being strongly dependent on the attitude of the satellite, the drag coefficient is also a function of ambient parameters like temperature and mean molecular mass as seen in Section II. The ambient parameters exhibit a diurnal variation and are also dependent on the location of the satellite. Therefore, as the satellite orbits from dayside to nightside and back, the drag coefficient exhibits a short period oscillation corresponding to the orbital motion of the satellite superposed on a long period oscillation corresponding to the diurnal variation. The period of the short period oscillation is equal to the orbital period of the satellite while the period of the long period oscillation is one day. There are some additional frequencies observed in the drag coefficient corresponding to the lat-long variation of the ambient parameters. The amplitude of the short period oscillations dominates over the others. In this case, using a body fixed Fourier model is not advantageous since these variations are independent of the attitude of the satellite. These periodic variations can be tied to the orbit itself since the periodicity is the same as that of the orbit. The Fourier expansion of the drag coefficient around the argument of latitude of the satellite (u) in its orbit is written as,

$$C_d = \sum_{n=0}^{\infty}(\bar{A}_n \cos nu + \bar{B}_n \sin nu). \tag{8}$$

Since the drag coefficient does not have an explicit dependence on the argument of latitude, finding the theoretical Fourier coefficients is difficult in this case. In order to find the nominal Fourier coefficients for the filter, a nonlinear least squares curve fitting is done on the drag coefficient variation in one orbit with the Fourier series model.

IV. SIMULATION SETUP

Before applying the Fourier series model on real data, it is tested on simulated examples based on actual satellites. A simplified force model is used to analyze the periodic and secular effects of the drag coefficient variation.

A. Force model

The force model used to generate the true trajectory comprises of the two body force and atmospheric drag. In order to isolate the effects of atmospheric drag, other perturbation forces are not included. The same force model is used in the filter as well. The two body and atmospheric drag accelerations are given by,

$$\boldsymbol{a_{two-body}} = -\mu_e \frac{\boldsymbol{r}}{r^3} \tag{9}$$

$$\boldsymbol{a_{drag}} = -\frac{1}{2}\rho C_d \frac{A_{ref}}{m} v_r^2 \hat{\boldsymbol{u}} \tag{10}$$

where $\boldsymbol{v_r}$ is the velocity of the satellite relative to the flow. NRLMSISE-00 is used to model the atmospheric density (ρ). The reference area used to normalize the drag coefficient is taken as 1. The satellite mass is assumed to be known.

B. Measurements

It is assumed that GPS measurements are sampled by the satellite every 10 s. Position and velocity in the earth fixed frame are given by an on-board GPS receiver. The true measurements are generated from the simulated trajectory in ECI frame with a simple frame rotation, given by,

$$\boldsymbol{y_{pos}} = \boldsymbol{R}^{ECI}_{ECEF}\boldsymbol{r} + \mathcal{N}(0, \sigma_p) \tag{11}$$

$$\boldsymbol{y_{vel}} = \boldsymbol{R}^{ECI}_{ECEF}\boldsymbol{v} + \dot{\boldsymbol{R}}^{ECI}_{ECEF}\boldsymbol{r} + \mathcal{N}(0, \sigma_v) \tag{12}$$

where $\sigma_p = 5m$ and $\sigma_v = 1mm/s$ are the measurement noise standard deviations in position and velocity.

V. SIMULATED EXAMPLES

In order to evaluate the Fourier model, two satellites in different orbital regimes are taken into consideration.

A. Case 1

A cubical satellite with a simple geometry at an altitude of around 600 km is considered for analysis. The initial orbital elements in order to simulate the truth are given in Table 2.

Element	Value
a	6971 km
e	0
i	97.8^0
Ω	0^0
u	0^0

Table 1 Initial orbital elements of first candidate satellite for truth generation

A simple shape model shown in Fig. 2 is considered to be able to use the physical model described in section II. A cubical shape with dimensions 60 cm x 60 cm x 60 cm is taken with the nadir face area double the rest of the faces due to the presence of an antenna on the nadir face. Shadowing and multiple reflections due to the antenna have not been considered. A diagonal inertia matrix with principal values $[3, 2.5, 5]\ kg.m^2$ is assigned. Since the physical model is dependent on the satellite surface mass, the satellite is assumed to be covered in Gallium Arsenide panels except the nadir face which is assumed to be made of Aluminum. The average satellite wall temperature is taken to be 300 K. Three modes of attitude stabilization are considered.

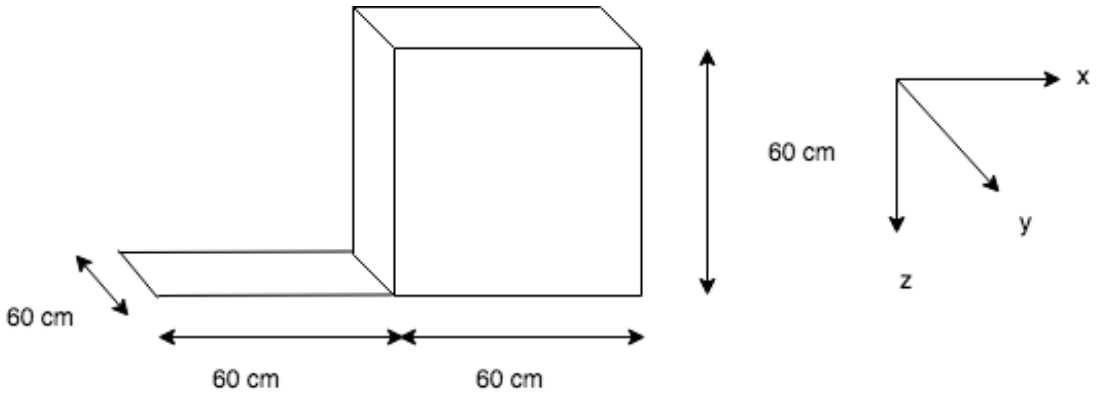

Fig. 2 Simplified shape model of the satellite

1) *Earth facing* - An Earth facing satellite will always have its leading face towards the flow. Therefore in a static atmosphere, the flow unit vector would be perpendicular to the satellite leading face resulting in a constant drag coefficient. The Fourier model will be equivalent to the cannonball drag coefficient in this case. But since the atmosphere is co-rotating with the Earth, there is be a periodic variation of the flow angle with the leading face which results in a small periodically varying component in the drag coefficient. The winds in the atmosphere contribute towards a random component in the drag coefficient variation but this has been ignored for the analysis at this stage.
2) *Random periodic slewing* - It is assumed that the satellite performs random slewing within a cone periodically, for say, imaging purposes. The satellite is taken to be nominally nadir pointing while slewing within a cone of 30^0 every 10, 20 and 30 minutes.
3) *Randomly tumbling satellite* - In order to study the performance of the Fourier model in an extreme case, a randomly varying attitude profile is taken. In order to simulate a separatrix motion, the angular velocity along the axis of intermediate inertia is taken to be the maximum.

B. Case 2

A satellite with fairly complex geometry at an altitude of 407 km is considered as the second case. The orbital regime is chosen due to the significant effects of drag experienced at such a low altitude.

Element	Value
a	6778 km
e	0
i	65^0
Ω	0^0
u	0^0

Table 2 Initial orbital elements of second candidate satellite for truth generation

It is assumed that the satellite consists of two large solar panels with area 16.45 m^2. In order to maximize solar power and minimize atmospheric drag, one solar panel is feathered to the flow while the other solar panel tracks the Sun. The feathered solar panel always contributes towards the tangential drag and hence it is added as a constant to the drag coefficient. The satellite bus is assumed to be fixed to the tracking solar panel and hence inertially stabilized. The areas of the satellite other than the feathered solar panel are taken to be 16.7, 12.3 and 18.1 m^2 in x, y and z respectively. Residual areas are added to account for protrusions etc. This is done in order to make the model asymmetric. Two attitude profiles are considered for analysis-

1) *Inertially stabilized* - The satellite is assumed to be inertially fixed with one solar panel always feathered to the flow. Therefore, the dominant variation of the flow direction is in the elevation angle (ϕ).

2) *Yaw maneuver* - It is assumed that the satellite performs a 180^0 yaw maneuver with a duration of half an orbit. This is a probable scenario when the spacecraft performs maneuvers for thermal control etc.
3) *Ambient parameter variations* - The drag coefficient being dependent on the ambient parameters is not constant throughout the orbit even when the flow vector remains constant. In order to analyze the diurnal variations in the drag coefficient, an Earth facing attitude profile is considered with a constant flow direction.

VI. RESULTS

The body fixed Fourier coefficients for both the simulated examples are found using the model in section III.A. The Fourier series is able to model the true drag coefficient as we go higher in the elevation order (O_ϕ) and azimuthal order (O_ϕ) which is expected. The difference between the true drag coefficients and the Fourier model for case 1 is plotted in Fig. 3. Due to the planes of symmetry in the satellite model in the first example, many of the Fourier coefficients turn out to be zero. In particular, all the B_{mn} coefficients are zero. D_{mn} is always zero for the physical model in section II. For A_{mn}, only the even elevation orders and multiples of four for the azimuthal orders are non-zero. In contrast, for the second example, most of the Fourier coefficients are non-zero. In both the examples, the variation of drag coefficient due to attitude is isolated from the variation due to ambient parameters and the latter is considered only for the Earth facing attitude profile in case 2. The results from the two simulation cases are outlined below. For all the cases, unless stated otherwise, the initial values for perturbations in the states and covariances for the filter are listed in Table 3. A batch filter is used to process the data of 10 orbits to evaluate the body fixed Fourier model and the states are then propagated for the next 40 orbits. In case 2 while evaluating the orbit fixed Fourier model, the data of 18 orbits is processed as explained later.

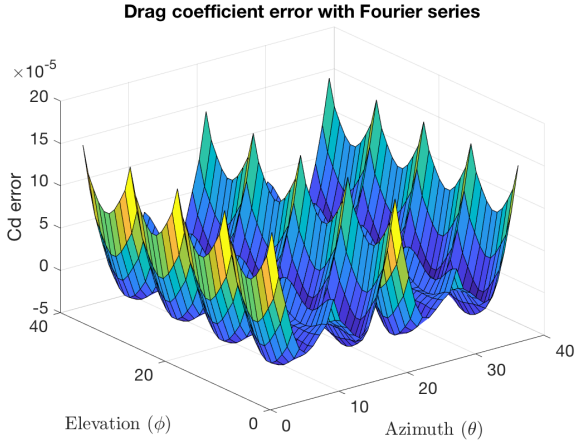

Fig. 3 Difference in the drag coefficients between the Fourier model of order 20 and the physical model for case 1

Parameter	Value
Position (x,y,z)	10 m
Velocity (x,y,z)	0.01 m/s
σ_{pos} (x,y,z)	10 m
σ_{vel} (x,y,z)	0.01 m/s

Table 3 Initial perturbations and standard deviation for the initial states in the filter

For the estimation of the Fourier coefficients in the filter, the nominal values are taken as the true values found using the models in III and the standard deviations are taken as the same order of magnitudes as the coefficient themselves. This is done so as to constrain the the magnitudes of the estimated coefficients and to prevent the filter from assigning large values to them. This problem is frequently encountered in gravitational field estimation [18].

A. Case 1

When the satellite is Earth facing, there's a very small periodic oscillation in the drag coefficient. The relative velocity vector varies in the range $[-3.8^0, 3.8^0]$ in θ while in ϕ, the variation is negligible. Therefore, the double Fourier series reduces to a single series in this case. As noted before, the Fourier coefficients are zero for azimuth till order 4. Therefore, only order 4 Fourier coefficient for θ is estimated along with the order 0 (cannonball) in the filter. As can be seen in Fig. 4 , the drag coefficient variation is very small due to the winds.

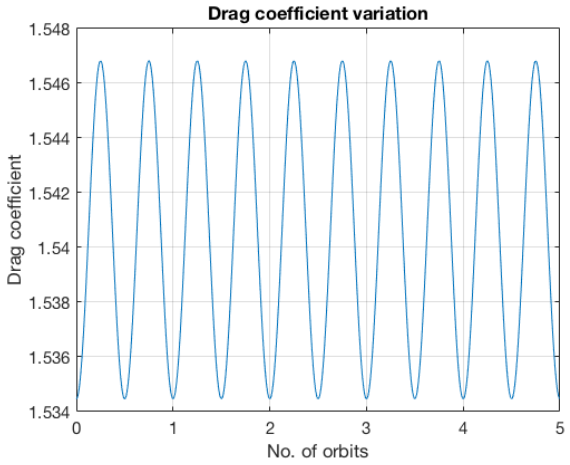

Fig. 4 Variation of drag coefficient for an earth facing satellite due to co-rotating atmosphere

The in-track error for the estimated trajectory is found as follows.

$$\delta I = a|u - \hat{u}| \tag{13}$$

where a is the nominal semi-major axis and u and $\hat{u}$ are the true and estimated argument of latitude respectively. The in-track error and altitude error between the order 0 and order 4 coefficients are plotted below.

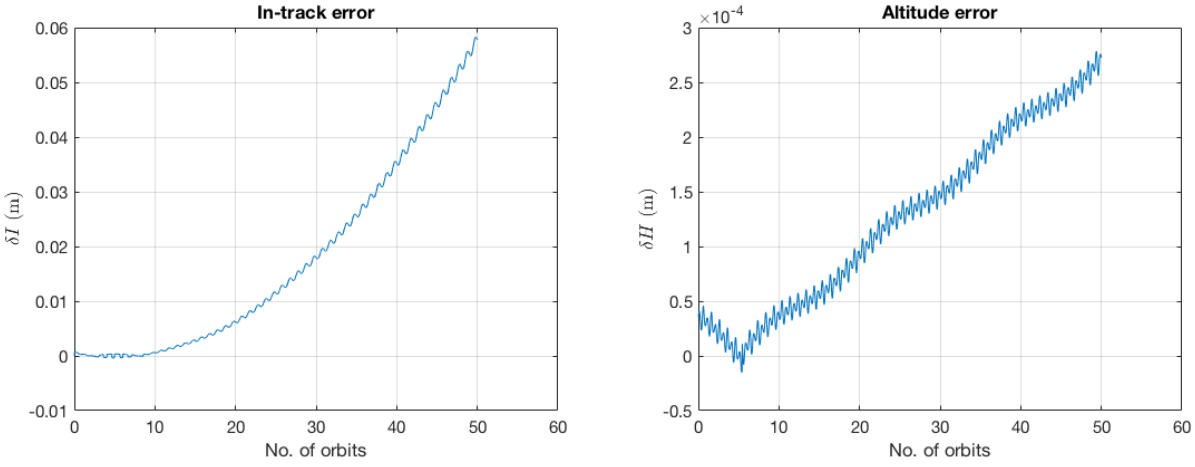

Fig. 5 In-track error (left) and altitude error (right) between order 0 and and order 4 Fourier models

It can be seen that the errors for the standard order 0 model are higher than order 4 model. The improvement with order 4 model is not significant since the drag coefficient variation is very small. But the results show the potential of a higher order Fourier model being able to capture variations in the drag coefficient due to attitude.

The second attitude profile considered is the periodic random slewing of the satellite within a cone of 30^0. Three different periods are considered for the variation - 10, 20 and 30 minutes in order to see if the Fourier model is able to capture variations of different frequencies. The drag coefficient variation for the 10 minute period slewing is plotted below.

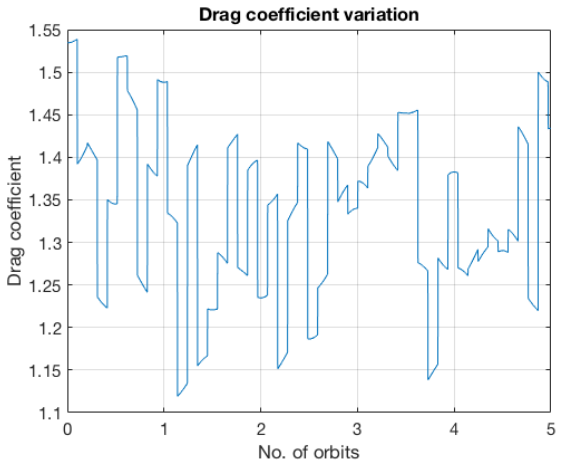

Fig. 6 Variation of drag coefficient for a satellite slewing within a cone of 30^0 every 10 minutes

In this case, since the drag coefficient varies in both elevation and azimuth, there are non-zero coefficients below order 4 which capture variations in elevation. But since the azimuth variation is not captured by the Fourier model until order 4, the results are worse than the standard cannonball for orders below 4. But there's a significant improvement on using the order 4 model. Such a trend is seen in all the frequencies considered. Therefore, for the periods of 20 and 30 minutes, only order 4 is compared to the order 0 model.

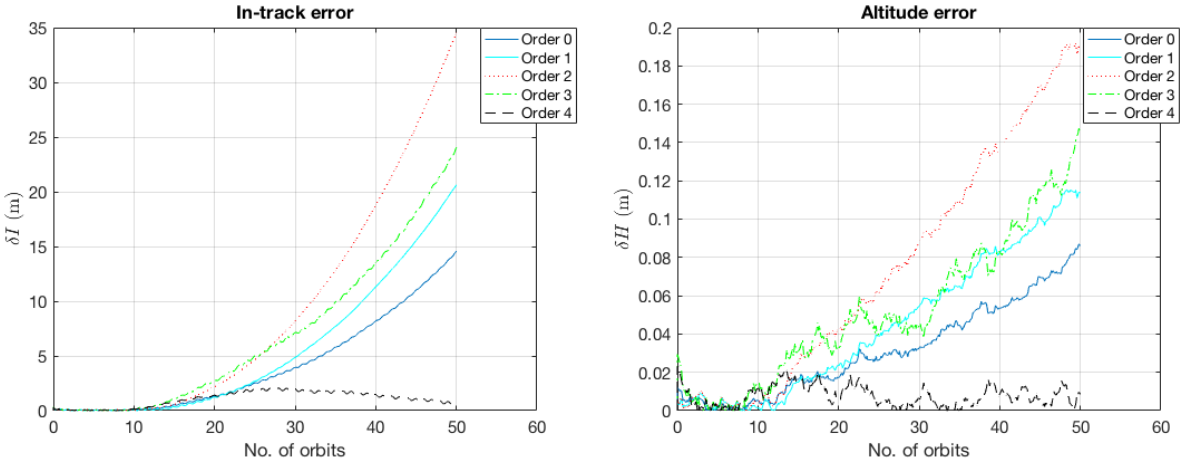

Fig. 7 In-track error (left) and altitude error (right) for a satellite slewing randomly within a 30^0 cone every 10 minutes

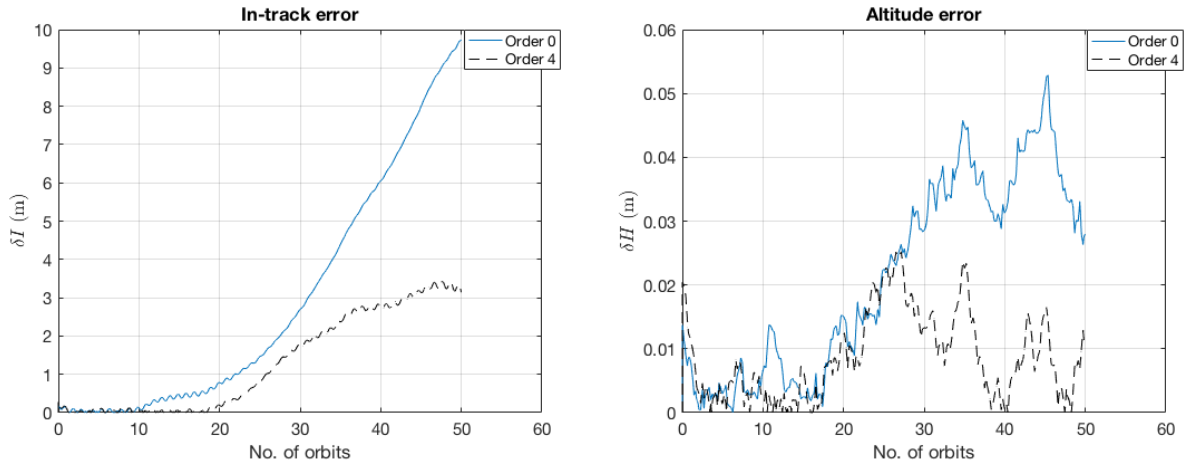

Fig. 8 In-track error (left) and altitude error (right) for a satellite slewing randomly within a 30^0 cone every 20 minutes

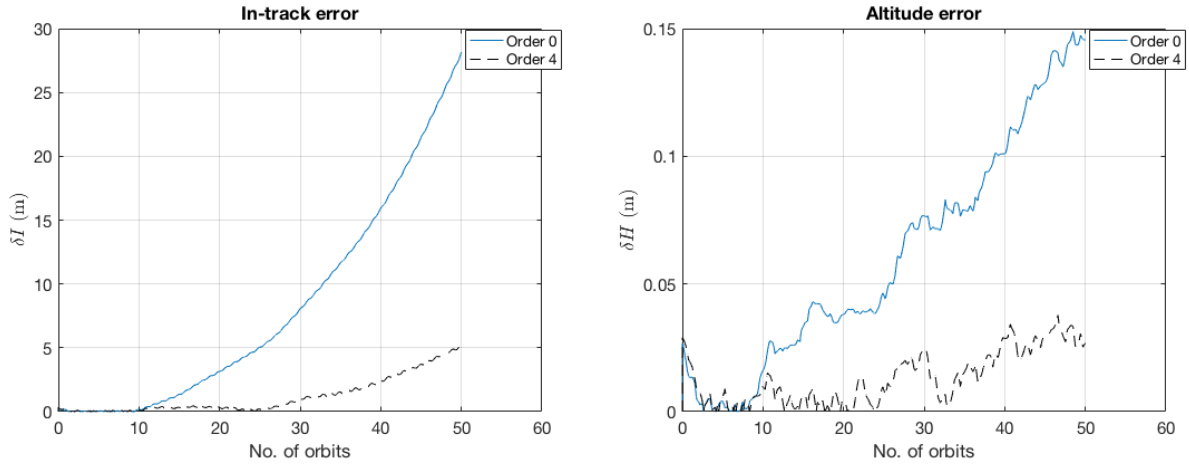

Fig. 9 In-track error (left) and altitude error (right) for a satellite slewing randomly within a 30^0 cone every 30 minutes

The third attitude profile considered for analysis is that of a randomly tumbling satellite. The initial Euler angles are taken to be 70^0 roll, 70^0 pitch and 70^0 yaw. The angular velocities along the x, y and z axes are taken to be $[0.1, 0.5, 0.1]^0/s$. The drag coefficient variation is plotted below.

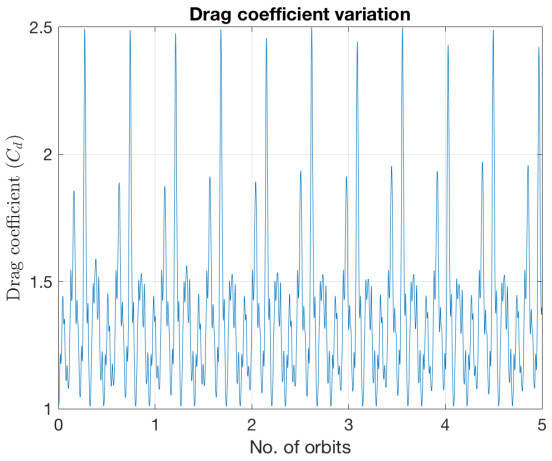

Fig. 10 Variation of drag coefficient for a randomly tumbling satellite

There's not a significant improvement in the errors with the order 4 Fourier model as can be seen in Fig. 11. Even with higher order coefficients, the improvement is the same. In this case, the drag coefficient mean is able to capture most of the variation.

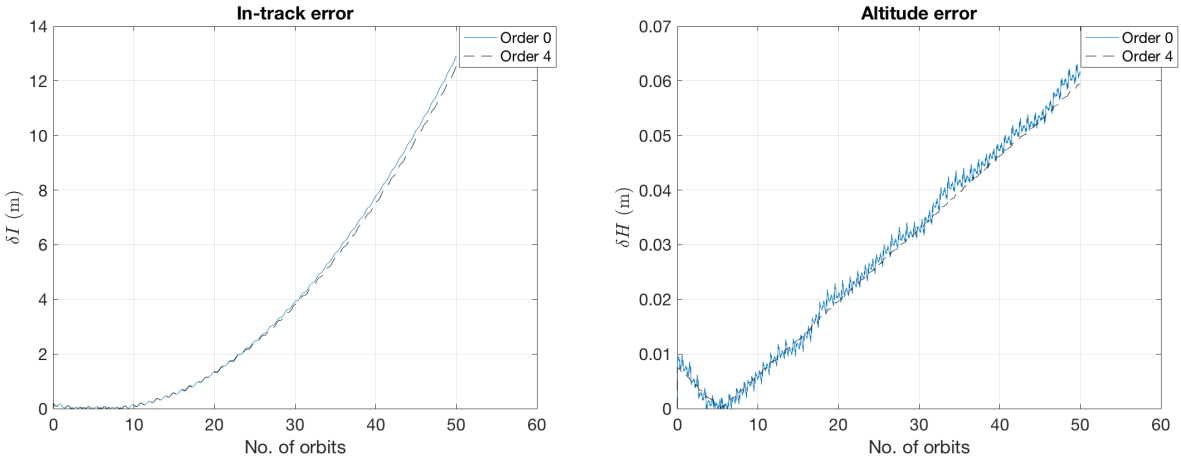

Fig. 11 In-track error (left) and altitude error (right) for a randomly tumbling satellite

B. Case 2

For an inertially stabilized attitude profile, the drag coefficient variation is essentially in the elevation direction. There's a small variation in the azimuth direction as seen in case 1. Due to the absence of planes of symmetry in this case, all the even A_{mn} coefficients for both the directions are non-zero. With the fixed box wing configuration, the drag coefficient is seen to vary periodically as seen in Fig. 12. It is important to note that the reference area in Eq. 10 is taken as 1 m^2 and hence the drag coefficient is normalized by an area of 1 m^2 which explains the large values of the drag coefficient. Generally, Cd values are normalized by a reference cross sectional area. But in the drag acceleration equation, the drag coefficient has to be multiplied with same reference area, so it can be taken to be any value.

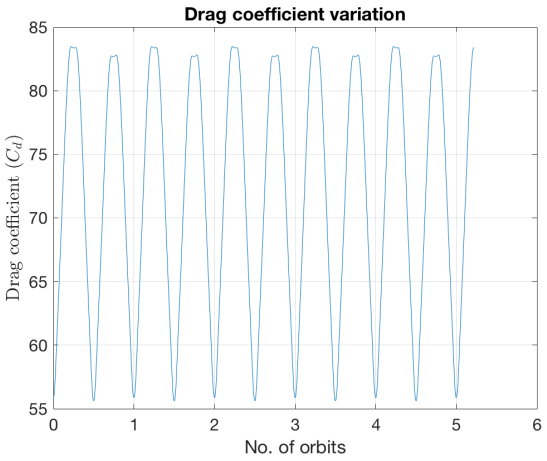

Fig. 12 Variation of drag coefficient for an inertially stabilized satellite

It is evident from Fig. 13 that all higher order Fourier models perform better than the order 0 model. But there's especially a significant improvement from order 1 to order 2. This can be explained by looking at the variation of the drag coefficient in Fig. 12. In each orbit, the drag coefficient varies almost periodically with a frequency twice that of the orbit period. Since the frequency of order 2 is twice the mean anomaly in this case, order 2 is able to capture the drag coefficient better than order 1.

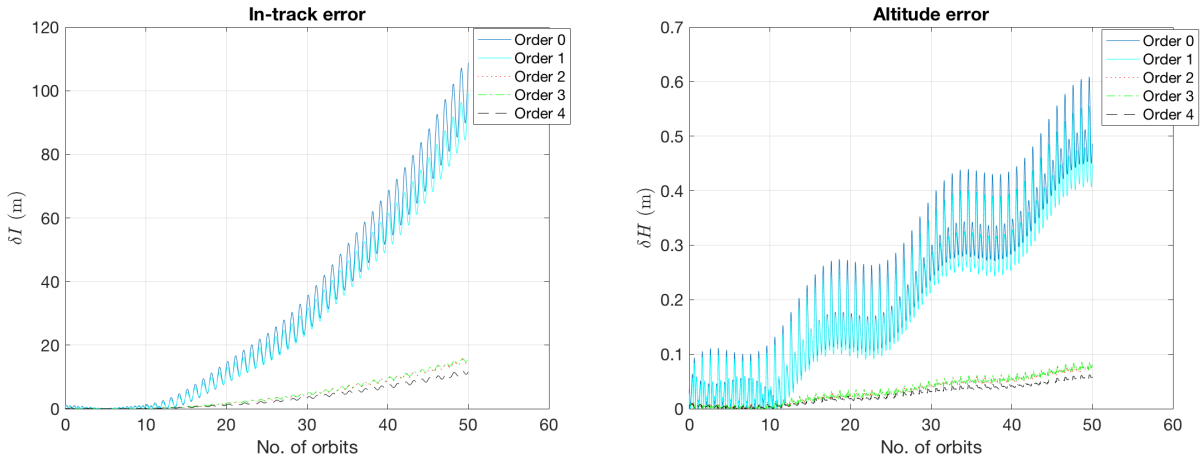

Fig. 13 In-track error (left) and altitude error (right) for an inertially stabilized satellite

If the varying cross-sectional area of the satellite is taken into account while estimating the drag coefficient, the in-track and altitude errors would improve over the order 0 model as seen in Fig. 14. But since the drag coefficient is not a simple scaling of the cross sectional area, the higher order Fourier models still perform better.

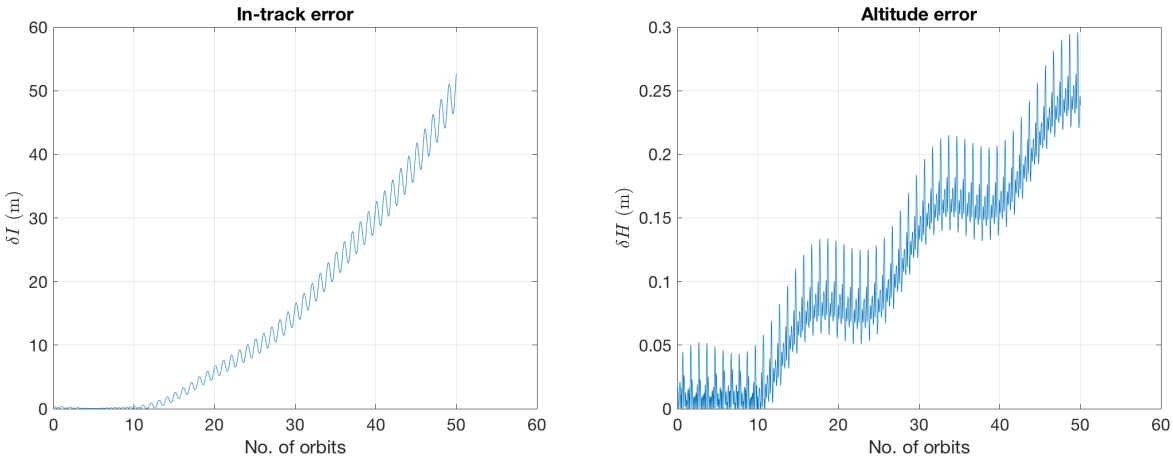

Fig. 14 In-track error (left) and altitude error (right) for an inertially stabilized satellite taking into account the varying cross sectional area

If the satellite performs an attitude maneuver, there would be a temporary aperiodic component introduced in the drag coefficient. In this case, there would be dominant components in the drag coefficient in both the directions for the duration of the maneuver. An example of a 180^0 yaw maneuver with a duration of half an orbit is analyzed. The drag coefficient variation is shown in Fig. 15

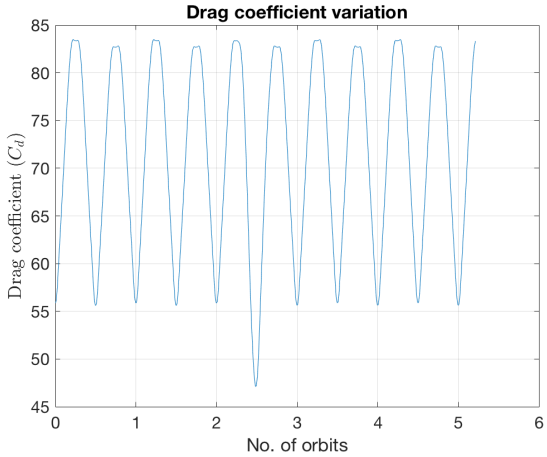

Fig. 15 Variation of drag coefficient for an inertially stabilized satellite with a short duration yaw maneuver

Only the even order models are compared with the order 0 model since they are expected to show a more significant improvement. As can be seen in Fig. 16, significant improvements are seen in the errors for higher even order models.

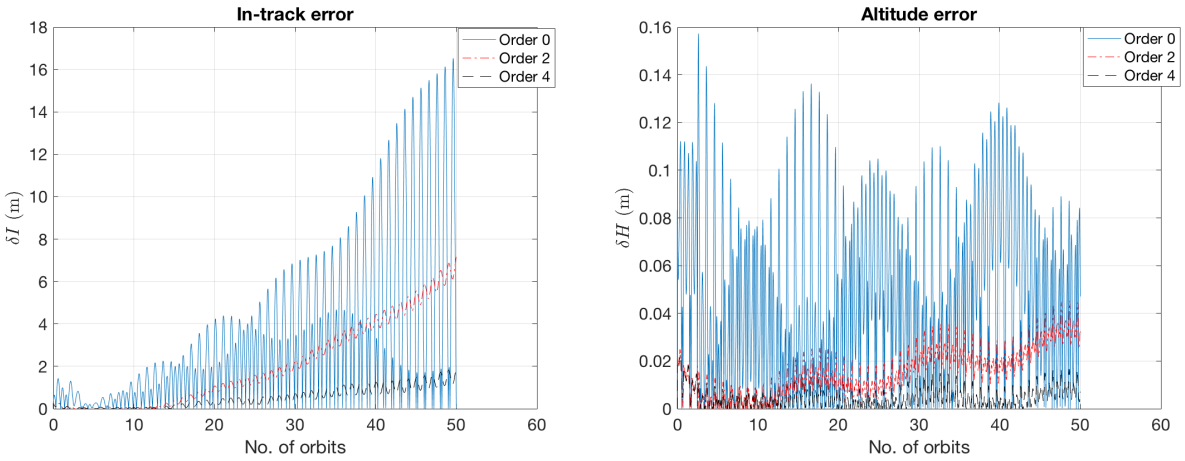

Fig. 16 In-track error (left) and altitude error (right) for an inertially stabilized satellite with a short duration yaw maneuver

The drag coefficient along with the attitude, is a function of the ambient parameters as well. Atmospheric parameters like temperature and mean molecular mass are dependent on the time of the day as well as the latitude, longitude and altitude. In all the above cases, these parameters were considered constant and the explicit dependence of the drag coefficient on the attitude was studied. In order to analyze the variation of drag coefficient solely due to ambient parameters, an Earth facing attitude profile with a constant flow vector is considered. The drag coefficient is shown in Fig. 17.

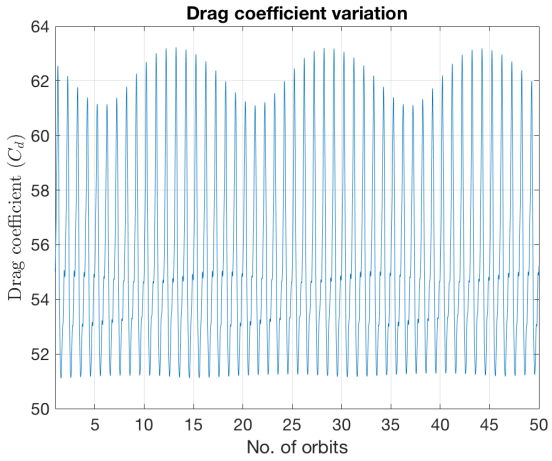

Fig. 17 Variation of drag coefficient for an Earth facing satellite due to ambient parameters

It can be seen that along with a periodicity of the drag coefficient in an orbit, there's a superposed trend with a period of around 18 orbits (1 day). This period is due to the diurnal variation of the ambient parameters. A curve fitting for the drag coefficient using the orbit fixed Fourier model is performed in order to find the nominal coefficients for the filter. In this case, the data for 18 orbits i.e. a complete day is processed by the filter since the mean can be captured only with a minimum of one day of data. The in-track and altitude errors for the higher order Fourier models are shown in Fig. 18. The improvement for all the higher order models is nearly the same and therefore not distinguishable in the figure.

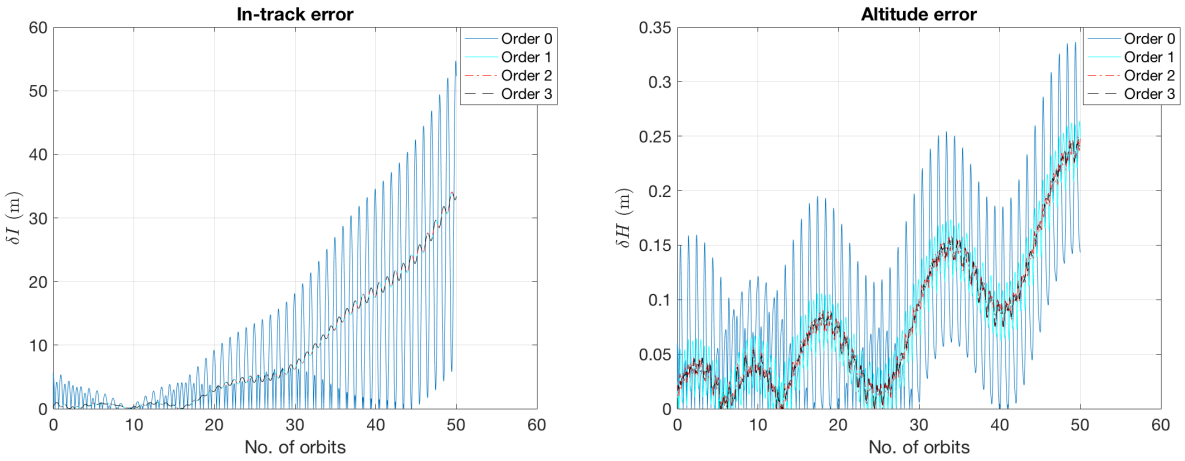

Fig. 18 In-track error (left) and altitude error (right) for an Earth facing satellite due to periodic variation of ambient parameters

VII. PRACTICAL APPLICATIONS

The body fixed Fourier model is applied to the orbit determination of a real low earth satellite in a ~407 km orbit. A batch filter is used to process the available on-board GPS receiver data. The satellite box is nadir pointing while the solar panel is tracking the sun and therefore exhibits an attitude profile periodic with the orbit. In order to process the in-orbit GPS data, realistic force models are required. The following forces are considered in the filter model

- 40x40 Earth's gravitational field (EGM-2008)
- Third body effects of Sun and Moon (DE-430 ephemerides)
- Solar radiation pressure (cannonball model)
- Atmospheric drag (Fourier model)

SPICE toolkit is used for the coordinate frame and time system conversions. A data arc of one day duration is processed using the batch filter. The state estimate at the end of one day is propagated to the end of the next day. The errors in the predicted residuals are defined with respect to the true GPS data. The difference in the errors in predicted residuals between the order 0 and order 4 models is plotted below.

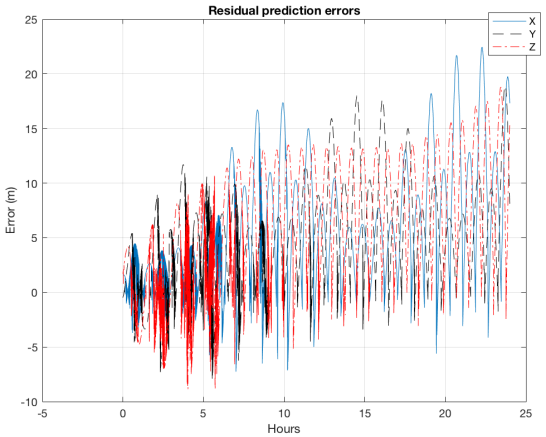

Fig. 19 Difference in the predicted residual errors between order 0 and order 4 Fourier models

It can be seen from Fig. 19 that the order 4 Fourier model shows potential of improvement over the constant drag coefficient model. But the improvement might also be due to presence of more parameters being estimated. The filter might be attributing errors from sources other than atmospheric drag to the coefficients, the Fourier model being

periodic with the orbit for the given attitude profile. The coupling between the various perturbing forces and the Fourier coefficients being estimated needs to be analyzed further.

VIII. CONCLUSIONS

In general, tracking the variations in the drag coefficient in the OD process is quite difficult due to its dependence on various satellite dependent and ambient parameters. Modeling the drag coefficient in terms of a Fourier series provides a simple way of estimating the drag coefficient due to the orthogonality of the Fourier coefficients. The body fixed Fourier coefficients significantly improve the position errors due to the attitude dependent variation of the drag coefficient. This is consistently seen in all the examples considered. The orbit fixed coefficients are able to capture the drag coefficient variation due to ambient parameters. In the inertially stabilized case, the body fixed coefficients reduce to the orbit fixed coefficients since the attitude varies at the same rate as the true anomaly. In all the simulations considered, ideal scenarios were taken with atmospheric drag being the only perturbation in the orbit. In reality, in the presence of other perturbing forces, the filter tries to capture the different error sources in the parameters being estimated. Therefore, the Fourier coefficients get coupled with perturbing forces other than atmospheric drag. The performance of the Fourier model in the presence of other forces is currently being investigated. A preliminary analysis with real GPS data from a low Earth orbit satellite shows potential of improved accuracy over the constant drag coefficient. Future work will focus on developing a common framework to capture the combined effects of the attitude and ambient parameters on the drag coefficient in a realistic scenario in the presence of other perturbing forces.

References

[1] Doornbos, E., "Thermospheric Density and Wind Determination from Satellite Dynamics," Ph.D. thesis, Delft University of Technology, 2011.

[2] Moore, P., "The Effect of Aerodynamic Lift on Near Circular Satellite Orbits," *Planetary Space Science*, Vol. 33, No. 5, 1985, pp. 479–491. doi:0032-0633/85.

[3] Vallado, D. A., and Finkleman, D., "A critical assessment of satellite drag and atmospheric density modeling," *Acta Astronautica*, Vol. 95, 2014, pp. 141–165. doi:10.1016/j.actaastro.2013.10.005.

[4] Emmert, J., "Thermospheric Mass Density: A Review ," *Advances in Space Research*, Vol. 56, 2015, pp. 773–824. doi: 10.1016/j.asr.2015.05.038.

[5] Lucchesi, D., "Reassessment of the Error Modelling of Nongravitational Perturbations on LAGEOS II and Their Impact in the Lense-Thirring Determination. Part I," *Planetary and Space Science*, Vol. 49, 2001, pp. 447–463. doi:10.1016/S0032-0633(00)00168-9.

[6] McMahon, J. W., and Scheeres, D. J., "Improving Space Object Catalog Maintenance Through Advances in Solar Radiation Pressure Modelling," *Journal of Guidance, Control, and Dynamics*, Vol. 38, No. 8, 2015, pp. 1366–1381. doi:10.2514/1.G000666.

[7] McMahon, J. W., and Scheeres, D. J., "New Solar Radiation Pressure Force Model for Navigation," *Journal of Guidance, Control, and Dynamics*, Vol. 33, No. 5, 2010, pp. 1418–1428. doi:10.2514/1.48434.

[8] Hesar, S. G., Scheeres, D. J., and McMahon, J. W., "Precise Solar Radiation Pressure Models for Small-Body Orbiters: Applications to OSIRIS-REx Spacecraft," *Journal of Guidance, Control, and Dynamics*, Vol. 40, No. 7, 2017, pp. 1638–1650. doi:10.2514/1.G002323.

[9] Hesar, S. G., Scheeres, D. J., and McMahon, J. W., "Precise Model for Small-Body Thermal Radiation Pressure Acting on Spacecraft," *Journal of Guidance, Control, and Dynamics*, Vol. 40, No. 10, 2017, pp. 2432–2441. doi:10.2514/1.G002566.

[10] Sentman, L., "Free Molecule Flow Theory and Its Application to the Determination of Aerodynamic Force," Lmsc-448514, ad 265-409, Lockheed Missiles and Space company, 1961.

[11] Schamberg, R., *A New Analytic Representation of Surface Interaction for Hyperthermal Free Molecular Flow*, Academic press, Santa Monica, California, 1959.

[12] Pardini, C., Anselmo, L., Moe, K., and Moe, M., "Drag and Energy Accommodation Coefficient During Sunspot Maximum," *Advances in Space Research*, , No. 45, 2010, pp. 638–650. doi:10.1016/j.asr.2009.08.034.

[13] Moe, M. M., Wallace, S. D., and Moe, K., "Recommended Drag Coefficients for Aeronomic Satellites," *The Upper Mesosphere and Lower Thermosphere: A Review of Experiment and Theory*, Vol. 87, 1995, pp. 349–356.

[14] Sutton, E. K., "Normalized Force Coefficients of Satellites with Elongated Shapes," *Journal of Spacecraft and Rockets*, Vol. 46, No. 1, 2009, pp. 112–116. doi:10.2514/1.40940.

[15] Moe, K., and Moe, M. M., "Gas Surface Interactions and Satellite Drag Coefficients," *Planetary and Space Science*, Vol. 53, No. 8, 2005, pp. 793–801. doi:10.1016/j.pss.2005.03.005.

[16] Pilinski, A. B. M., Marcin D., and Palo, S. E., "Semi-Empirical Satellite Accommodation Model for Spherical and Randomly Tumbling Objects," *Journal of Spacecraft and Rockets*, Vol. 50, No. 3, 2013, pp. 556–571. doi:10.2514/1.A32348.

[17] Poularikas, A., *The Handbook of Formulas and Tables for Signal Processing*, CRC Press LLC, Boca Raton, 1999.

[18] Scheeres, D., Hesar, S., Tardivel, S., Hirabayashi, M., Farnocchia, D., McMahon, J., Chesley, S., Barnouin, O., Binzel, R., Bottke, W., Daly, M., Emery, J., Hergenrother, C., Lauretta, D., Marshall, J., Michel, P., Nolan, M., and Walsh, K., "The geophysical environment of Bennu," *Icarus*, , No. 276, 2016, pp. 116–140. doi:10.1016/j.icarus.2016.04.013.